Molecular Therapy
Original Article

MiR126-targeted-nanoparticles combined with PI3K/AKT inhibitor as a new strategy to overcome melanoma resistance

Maria Beatrice Arasi,[1] Gabriele De Luca,[1] Laura Chronopoulou,[2,3] Francesca Pedini,[1] Eleonora Petrucci,[1] Michela Flego,[4] Annarita Stringaro,[5] Marisa Colone,[5] Luca Pasquini,[6] Massimo Spada,[7] Valentina Lulli,[1] Maria Chiara Perrotta,[2] George Adrian Calin,[8,9] Cleofe Palocci,[2,3] Mauro Biffoni,[1] Federica Felicetti,[1,10] and Nadia Felli[1,10]

[1]Department of Oncology and Molecular Medicine, Istituto Superiore di Sanità, Viale Regina Elena 299, 00161 Rome, Italy; [2]Department of Chemistry, Sapienza University of Rome, P.le A. Moro 5, 00185 Rome, Italy; [3]Research Center for Applied Sciences to the safeguard of Environment and Cultural Heritage (CIABC) Sapienza University of Rome, P.le A. Moro 5, 00185 Rome, Italy; [4]National Center for Global Health, Istituto Superiore di Sanità, Viale Regina Elena 299, 00161 Rome, Italy; [5]National Center for Drug Research and Evaluation, Istituto Superiore di Sanità, Viale Regina Elena 299, 00161 Rome, Italy; [6]Core Facilities, Istituto Superiore di Sanità, Viale Regina Elena 299, 00161 Rome, Italy; [7]Center of Animal Research and Welfare, Istituto Superiore di Sanità, Viale Regina Elena 299, 00161 Rome, Italy; [8]Translational Molecular Pathology, MD Anderson Cancer Center, Texas State University, 1515 Holcombe Blvd, Houston, TX 77030, USA; [9]The RNA Interference and Non-coding RNA Center, MD Anderson Cancer Center, Texas State University, Houston, 1515 Holcombe Blvd, Houston, TX 77030, USA

Metastatic melanoma poses significant challenges as a highly lethal disease. Despite the success of molecular targeting using $BRAF^{V600E}$ inhibitors (BRAFis) and immunotherapy, the emergence of early recurrence remains an issue and there is the need for novel therapeutic approaches. This study aimed at creating a targeted delivery system for the oncosuppressor microRNA 126 (miR126) and testing its effectiveness in combination with a phosphatidylinositol 3-kinase (PI3K)/ protein kinase B (AKT) inhibitor for treating metastatic melanoma resistant to BRAFis. To achieve this, we synthesized chitosan nanoparticles containing a chemically modified miR126 sequence. These nanoparticles were further functionalized with an antibody specific to the chondroitin sulfate proteoglycan 4 (CSPG4) melanoma marker. After evaluation *in vitro*, the efficacy of this treatment was evaluated through an *in vivo* experiment using mice bearing resistant human melanoma. The co-administration of miR126 and the PI3K/AKT inhibitor in these experiments significantly reduced tumor growth and inhibited the formation of liver and lung metastases. These results provide evidence for a strategy to target an oncosuppressive nucleic acid sequence to tumor cells while simultaneously protecting it from plasma degradation. The system described in this study exhibits encouraging potential for the effective treatment of therapy-resistant metastatic melanoma while also presenting a prospective approach for other forms of cancer.

INTRODUCTION

Melanoma is a neoplasia that arises from the malignant transformation of melanocytes, pigmented cells found in the basal layer of the epidermis.[1] There are approximately 300,000 new cases and 60,000 deaths worldwide each year. Melanoma incidence is rapidly increasing, with a 75% increase over the last 30 years.[2] It is noteworthy that both incidence and mortality of melanoma vary among different countries, with higher rates in Australia, New Zealand, Europe, and Northern America, associated with ethnicity, lifestyle, and genetic background.[3] Over the past decade, new therapeutic strategies have achieved greater efficacy and fewer side effects against late-stage melanoma.[4] Molecular analysis of the mechanisms leading to the transformation of melanocytes into melanoma cells has highlighted recurrent activating mutations in BRAF, which are present in more than 50% of cutaneous melanomas. The most common mutation found in melanoma (90%) is the V600E,[5] and significant advancements in the treatment of metastatic melanoma have been achieved by utilizing drugs targeting this mutated form of BRAF ($BRAF^{V600E}$), such as vemurafenib or dabrafenib. Response to BRAF inhibition usually has a short duration and is prolonged when combined with MEK (Mitogen-activated ERK kinase) inhibitors such as trametinib or binimetinib.[6–8] Despite the impressive results achieved in patients after treatment with these drugs, the early recurrence resistant to treatments remains the main limitation of this therapeutic strategy.[9–12] The recent use of immunological checkpoint inhibitors (ICIs) in advanced melanoma therapy is leading to a significant improvement in the prognosis of patients with metastatic melanoma. Although approximately 40% of patients show a good response, a significant number of patients still exhibit no initial

Received 30 May 2023; accepted 17 November 2023;
https://doi.org/10.1016/j.ymthe.2023.11.021.

[10]These authors contributed equally

Correspondence: N. Felli, Department of Oncology and Molecular Medicine, Istituto Superiore di Sanità, Viale Regina Elena 299, 00161 Rome, Italy.
E-mail: nadia.felli@iss.it

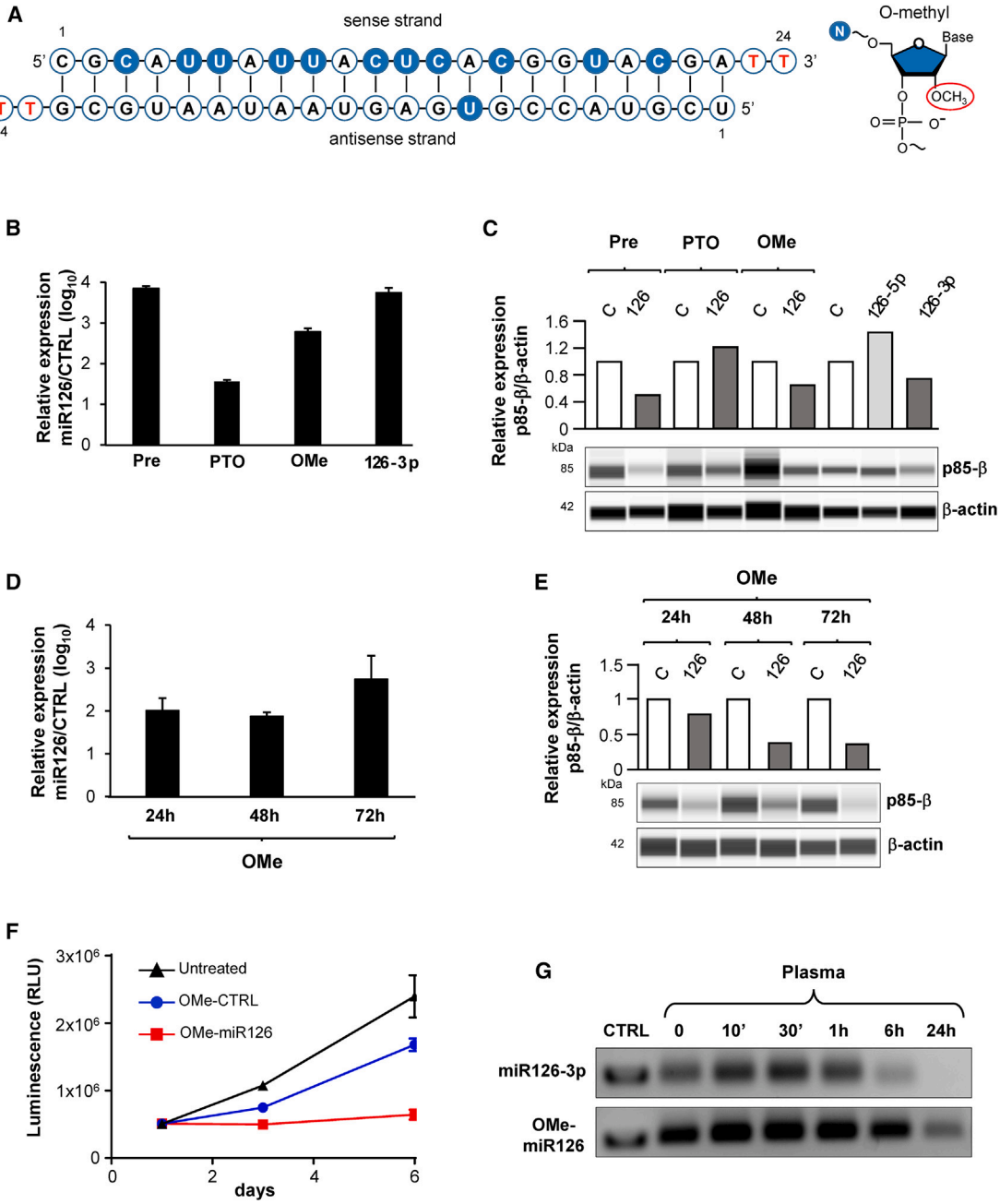

Figure 1. Chemical changes within the OMe-miR126 sequence: a comparative analysis of its function and stability in plasma

(A) OMe-miR126 consists of a double-stranded ribonucleotide and the anti-sense strand contains mature miR-126-3p sequence. All the pyrimidine residues of the sense strand and one of the uridine residues in the anti-sense strand are modified by O-methylation at the 2′-O pentose (2′-OMe). The sense and anti-sense strands have been modified with the addition of two 2′-deoxythymidine residues at the 3′ terminal of each strand. (B) Analysis of miR126 expression obtained by qRT-PCR performed 24 h after transfection of A375M-VR cell line with Pre-miR126 (Pre), PTO-miR126 (PTO), OMe-miR126 (OMe), and relative negative control. U6 snRNA was used as normalizer. The histogram columns represent the ratio ± SD of the values obtained from transfection of miR126 sequences and their respective controls. Commercial miR126-3p was used as positive reference. (C) WES analysis of p85-β protein in A375M-VR cell line after transfection with Pre-miR126, PTO-miR126, OMe-miR126 sequences or their relative negative controls. MiR126-3p and -5p were used as positive and negative references, respectively. β-Actin was utilized as internal loading control. (D) Analysis of miR126 expression in A375M-VR by qRT-PCR, performed 24, 48, and 72 h after OMe-miR126 internalization. Relative miR126 expression level was normalized on U6 snRNA. The

(legend continued on next page)

response to therapy. Therefore, new drugs are needed to improve melanoma treatment.[10] To address this problem, new combinations to inhibit various crucial pathways for tumor cell survival are under evaluation e.g., the simultaneous inhibition of mitogen-activated protein kinase (MAPK)/extracellular signal-regulated kinase (ERK) and phosphatidylinositol 3-kinase (PI3K)/protein kinase B (AKT) pathways.[13] Accumulating evidence suggests that non-coding RNAs (ncRNAs) play important roles in all key cellular processes. MicroRNAs (miRs) are small, highly conserved ncRNAs involved in the regulation of gene expression. In particular, miR126 acts as a tumor suppressor in several types of cancer.[14,15] A recent study has demonstrated a correlation between miR126 expression and the overall survival (OS) of melanoma patients. Specifically, it was found that melanoma patients with high miR126 expression had a significantly longer OS compared to those with low miR126 expression.[16] Consistent with this finding, our group and another research team have independently shown the anti-tumoral effects of miR126 on human metastatic melanoma cells. These effects are achieved through the repression of several key oncogenic molecules, including the regulatory subunit p85-β of the PI3K/AKT pathway, either directly or indirectly. More recently, we demonstrated that PIK-75 (a molecule that inhibits the PI3K/AKT regulatory subunit, p110α) was one of the most active among the 349 molecules in inhibiting the proliferation of metastatic melanoma cells.[17–20] We also demonstrated that the forced expression of miR126 significantly increased PIK-75 activity when used as a single agent or in combination with vemurafenib or dabrafenib. Interestingly, PIK-75 has been shown to be effective against early-passage cell lines derived from patient biopsies and melanoma cell lines resistant to either vemurafenib or dabrafenib, suggesting that it has the potential to overcome drug resistance.[17] The use of nucleic acids, including miRs, in therapy involves the need to overcome certain difficulties, especially related to their serum instability.[18] The aim of our work was to study a system to deliver miR126 directly to metastatic melanoma cells *in vivo*. An effective strategy in addressing these critical issues is the use of nanoparticles (NPs), thanks to their capacity to entrap and successively release drugs, excellent availability and biocompatibility, good stability, and enhanced drug solubility in body fluids.[19,20] Indeed, advances in nanotechnology have opened up new opportunities for nanomaterials, which offer distinct bioactivity due to their nanoscale properties, high surface area, and precise nanostructure.[21] Among various types of NPs, we selected NPs of chitosan (NP-CSs) because of their positive charge, which fosters drug loading and delivery efficiency, making them effective candidates for both passive and active drug delivery systems in cancer therapy.[22,23] We then functionalized NP-CSs to deliver them directly to metastatic melanoma cells by conjugation with an antibody moiety against a melanoma marker, CSPG4, which is overexpressed in several tumors, including melanoma. It plays a crucial role in cancer growth and was previously studied as a potential target of monoclonal antibodies (mAbs) or chimeric antigen receptor (CAR) T cells across different tumor types.[24]

RESULTS

To highlight the correlation between high expression of miR126 and increased survival of melanoma patients, as previously reported by Lin et al.,[16] we conducted a Kaplan-Meier analysis for OS using data from The Cancer Genome Atlas (TCGA) melanoma dataset (https://www.cancer.gov/ccg/research/genome-sequencing/tcga). TCGA Melanoma patient cohort, obtained from Xena data portal (https://xenabrowser.net/datapages/), were stratified into two groups based on their miR126-3p expression levels: high expression and low expression, by using UCSC Xena data portal (https://xenabrowser.net/datapages/) The analysis reaffirmed that the group with high miR-126-3p expression exhibited a significant improvement in OS ($p = 0.0199$, log rank test = 5.417) (Figure S1). Based on these findings and considering the proven anti-neoplastic role of miR126 in human melanoma,[17,25–27] we planned to evaluate the above reported specific miR sequence in an *in vivo* mouse model for the treatment of drug-resistant melanoma. RNA oligonucleotides in serum are susceptible to degradation by nucleases and have limited cellular uptake when introduced into living organisms. To overcome this problem, we synthesized three different miR126 sequences with specific chemical properties. In particular, we synthetized: a ∼70-nt precursor RNA molecule of miR126, without modifications (Pre-miR126), and its relative scramble sequence (Pre-CTRL);[28] a 27-nt sequence including a stabilized phosphorothioate double-stranded mature miR126-3p (PTO-miR126) and its relative negative control (PTO-CTRL)[29] (Table S1). Taking as a model the modifications made to a nucleotide sequence used for an approved drug,[30,31] we generated a sequence with all of the pyrimidines in the sense strand and one of the uridines in the anti-sense by adding a methyl group (CH_3) at the 2′-O position of the pentose (2′-OMe), thus increasing its thermal stability. In addition, two 2′-deoxythymidine nucleotide overhangs at their respective 3′ ends have been added to protect this molecule from nuclease cleavage (OMe-miR126) (Figure 1A; Table S1). The same modifications have been made to a negative control sequence (OMe-CTRL) (Table S1). To select the most effective sequence among them, we first evaluated their ability to inhibit the expression of PIK3R2 (p85-β) subunit of PI3K, a direct target of miR126-3p.[26,32] Specifically, we transfected A375M cells made resistant to vemurafenib (A375M-VR) with Pre-miR126, PTO-miR126, OMe-miR126, or their negative controls. Commercial miR126-3p and miR126-5p (hereafter indicated as miR126-3p and miR126-5p) have been used as positive and negative references, respectively.[26] In spite of ∼10 times lower expression levels of OMe-miR126 than Pre-miR126 or miR126-3p, as assessed by qRT-PCR (Figure 1B), immunoblotting analysis showed a similar p85-β reduction (50%–40%), whereas no reduction was observed using PTO-miR126 and, as expected, for miR126-5p (Figure 1C). Based on this evidence, we focused our efforts on OMe-miR126 as the most

histogram columns represent the ratio ± SD of the values obtained from transfection of miR126 sequences and their respective controls. (E) WES analysis of p85-β protein in A375M-VR, performed at 24, 48, and 72 h after transfection of OMe-miR126 or control sequence. β-Actin was utilized as internal loading control. (F) Cell Titer-Glo viability assay in untreated A375M-VR cells or after transfection with OMe-miR126 or relative negative control. Each transfected cell line was analyzed in triplicate. (G) Analysis of naked OMe-miR126 stability compared to commercial miR126-3p until 24 h of incubation in PBS containing 50% of human plasma at 37°C.

effective sequence. After a transient transfection of A375M-VR with this oligo (Figure 1D), we observed a significant p85-β down-modulation (Figure 1E) and a marked cell growth inhibition (Figure 1F). As a preparatory test for *in vivo* experiments, we evaluated the stability of OMe-miR126 and miR126-3p sequences in PBS containing 50% human plasma at 37°C. The time courses reported in Figure 1G show that, starting from the same quantity of OMe-miR126 and miR126-3p oligos, after 6 h of incubation, no reduction and a reduction to one-third was observed, respectively. Furthermore, a complete degradation of miR126-3p was observed after 24 h while OMe-miR126 was still clearly visible (∼80% of the initial quantity). To verify the lifetime of OMe-miR126, we extended the incubation to 48 h showing its complete degradation (not shown). The results described so far show that the chemical changes introduced in miR126-3p canonical sequence to obtain OMe-miR126 do not change its functionality and make it much more stable than the other sequences in the presence of plasma.

OMe-miR126 sequence in combination with BRAF inhibitors

We already demonstrated the efficacy of miR126 in combination with BRAF/ERK and PI3K/AKT inhibitors (vemurafenib and PIK-75, respectively).[17] Based on these results, we evaluated the cell growth inhibitory effect of the OMe-miR126 sequence on cell lines from metastatic melanoma (A375M and SKMEL28) and their sub-lines resistant to dabrafenib (A375M-DR and SKMEL28-DR), which were generated by culturing parental cells in increasing concentrations of drug. In A375M (Figure 2A, upper panel), in agreement with previous data, the half maximal inhibitory concentration (IC_{50}) of vemurafenib, dabrafenib, and PIK-75 were reduced by half when the treatments were combined with OMe-miR126, in comparison with OMe-CTRL sequence (from 704.7, 41, and 73.5 nM to 329.6, 22.3, and 40.3 nM, respectively). The same trend of IC_{50} values was observed in the combined treatments (vemurafenib + PIK-75) or (dabrafenib + PIK-75) with OMe-miR126, in comparison with OMe-CTRL sequence (from 56.7 and 30.4 nM to 34.4 and 12.7 nM, respectively). The excess over bliss values (EOB) indicated that OMe-miR126 was synergistic with each single drug (vemurafenib, dabrafenib, or PIK-75) or with their combination (vemurafenib + PIK-75 or dabrafenib + PIK-75) (Figure 2A, lower panel). Similar results were observed with the SKMEL28 cell line. The OMe-miR126 sequence reduced the IC_{50} values both in the presence of dabrafenib and PIK-75 alone (from 37 and 134.5 nM to 23.4 and 106 nM, respectively), as well as in the combined treatment (115 vs. 105 nM). A strong synergy between OMe-miR126 and dabrafenib was indicated from EOB index (Figure 2B). As reported in Figure 2C (left panel), in A375M-DR the IC_{50} of PIK-75 decreased from 153.3 to 120.5 nM and the EOB index highlights their synergy (Figure 2C, right panel). For SKMEL28-DR, we observed a marked IC_{50} decrease (318 vs. 213.4 nM), as reported in Figure 2D, but no synergistic effect was observed.

Synthesis of NP-CSs entrapping OMe-miR126 and NP-CSs entrapping OMe-CTRL

After confirming the functionality of the OMe-miR126 sequence, we focused on the potential utilization of targeted NP-CSs for the direct delivery of OMe-miR126 to melanoma cells. Previous studies[33–35] reported that morphology, net charge, and size of polyplexes are mainly determined by the amine groups/phosphate groups (N/P) ratio. It has been demonstrated that, using N/P ratios between 5 and 10, size and charge values are almost constant. In this case, for the same N/P ratio, by using lower-molecular-weight chitosan, a rapid release of loaded nucleic acid occurs, therefore obtaining less stable systems. Lavertu et al. demonstrated that, by increasing the N/P ratio from 5 to 10 (at fixed deacetylation degree), a lower molecular weight was required to achieve efficient stabilization of complexes, probably due to the stabilizing effect obtained by increasing the chitosan concentration.[36] Moreover, better transfection efficiency was obtained using an N/P ratio of 10. For these reasons, all chitosan NPs have been prepared with 50-kDa chitosan with an N/P ratio of 10.

NP-CSs were conjugated with a single-chain fragment variable (scFv) including the variable heavy chain (VH) and the variable light chain (VL) of the murine mAb 9.2.27 specific for the melanoma marker CSPG4 (anti-CSPG4) and a 6His tag.[37,38] The purified anti-CSPG4 was detected in a western-blot experiment with horseradish peroxidase (HRP)- conjugated anti-6His mAb (Figure 3A and section "materials and methods"). To evaluate the binding capacity of this anti-CSPG4 toward its target antigen, an immunofluorescence assay was performed by flow cytometry on A375M-DR melanoma and 293FT cell lines, expressing high and low levels of surface antigen CSPG4, respectively. The results obtained showed that this antibody can selectively interact with CSPG4 membrane receptor (Figure S2A). To evaluate the potential function of the soluble anti-CSPG4, we performed *in vitro* treatments of A375M-DR with increasing quantities of this soluble protein and no effect was observed up to 1 μg/mL (data not shown).

NP-CSs entrapping OMe-miR126 or OMe-CTRL (CS126s and CS-CTRLs, respectively) and surface conjugated with antibodies against the CSPG4 marker (Ab-CS126s and Ab-CS-CTRLs, respectively) were prepared and characterized as reported in Figure S2B. To synthesize Ab-CS126, in order to determine the suitable amount of antibody binding, different scFv:CS weight ratios were studied (Figure S2C). The amount of conjugated single-chain antibody, expressed as a percentage, was higher than 80% for all the scFv:CS ratios used. We used an intermediate scFv:CS weight ratio of 1:10 for all subsequent studies.

Physicochemical characterization of CS126 and Ab-CS126

Nanosight analysis was conducted to determine the dimensional distribution and NP concentration of CS126s, Ab-CS126s, and their respective controls. The results showed dimensions ranging from 112.6 ± 4.2 nm to 146.8 ± 6.9 nm for all types of NPs and an average particle concentration of 2.2×10^{11} NPs/mL and 1.7×10^{10} NPs/mL for CS126s/CS-CTRLs and Ab-CS126s/Ab-CS-CTRLs, respectively (Figure 3B). A physico-chemical characterization of CS126s and Ab-CS126s was also performed using DLS (dynamic light scattering), which roughly confirmed the dimensions obtained with Nanosight. The average polydispersion index (PDI) for all NP samples was 0.2, indicating a good quality of colloidal NPs. CSs are generally

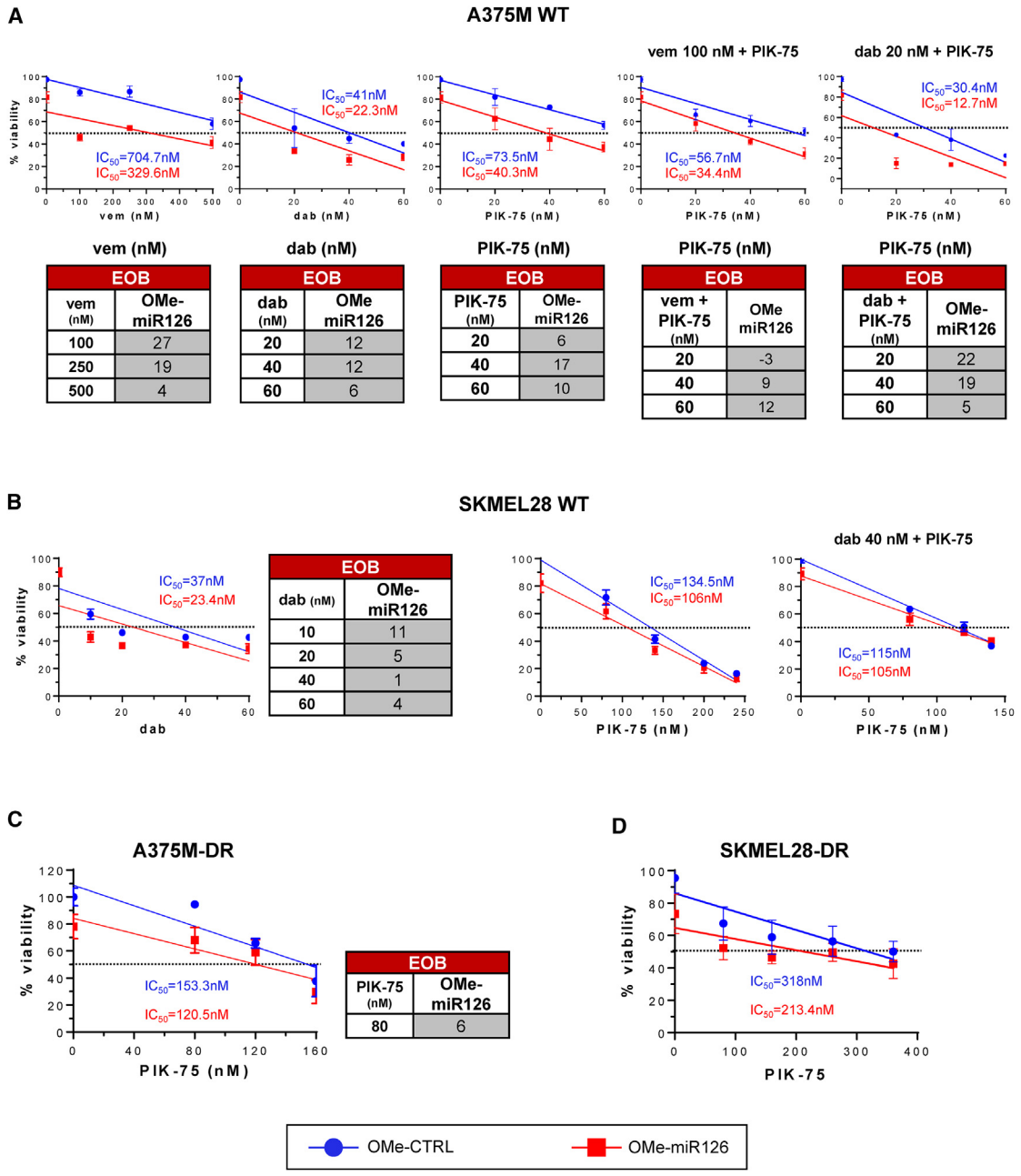

Figure 2. Analysis of melanoma cell line growth following treatment with OMe-miR126, BRAF, and PI3K inhibitors

(A) Cell growth inhibition mediated by OMe-miR126 sequence compared to OMe-CTRL in combination with vemurafenib, dabrafenib, PIK-75, vemurafenib + PIK-75, and dabrafenib + PIK-75 in A375M wild-type (WT) cell line (upper panel). Evaluation of excess over bliss values (EOB) for each condition in A375M WT (bottom panel). (B) Cell growth inhibition with the same sequences with dabrafenib, PIK-75, and dabrafenib + PIK-75. EOB in SKMEL28 WT. (C) Cell growth inhibition mediated by OMe-miR126 sequence and OMe-CTRL in combination with PIK-75 in A375M-DR cell line and relative EOB values. (D) Cell growth inhibition in SKMEL28-DR cell line. EOB indicates synergism >0, independent = 0, antagonism <0. Means ± SD of almost three experiments are reported.

characterized by a positive surface charge, due to the presence of amino groups that are positively charged at acidic pH. The positive charge is considered optimal for nanovector internalization within cells, as cellular membranes exhibit a negative charge.[39,40] As shown in Figure S2D, the average ζ-potential value was +37.8 ± 4.3 mV for CS126s and +33.3 ± 1.2 mV for Ab-CS126s. Scanning electron microscopy (SEM)/transmission electron microscopy (TEM) analyses were then performed to better characterize NP-CSs' morphology. As shown in Figure 3C, the dimensions appear smaller than those detected by DLS, as expected.

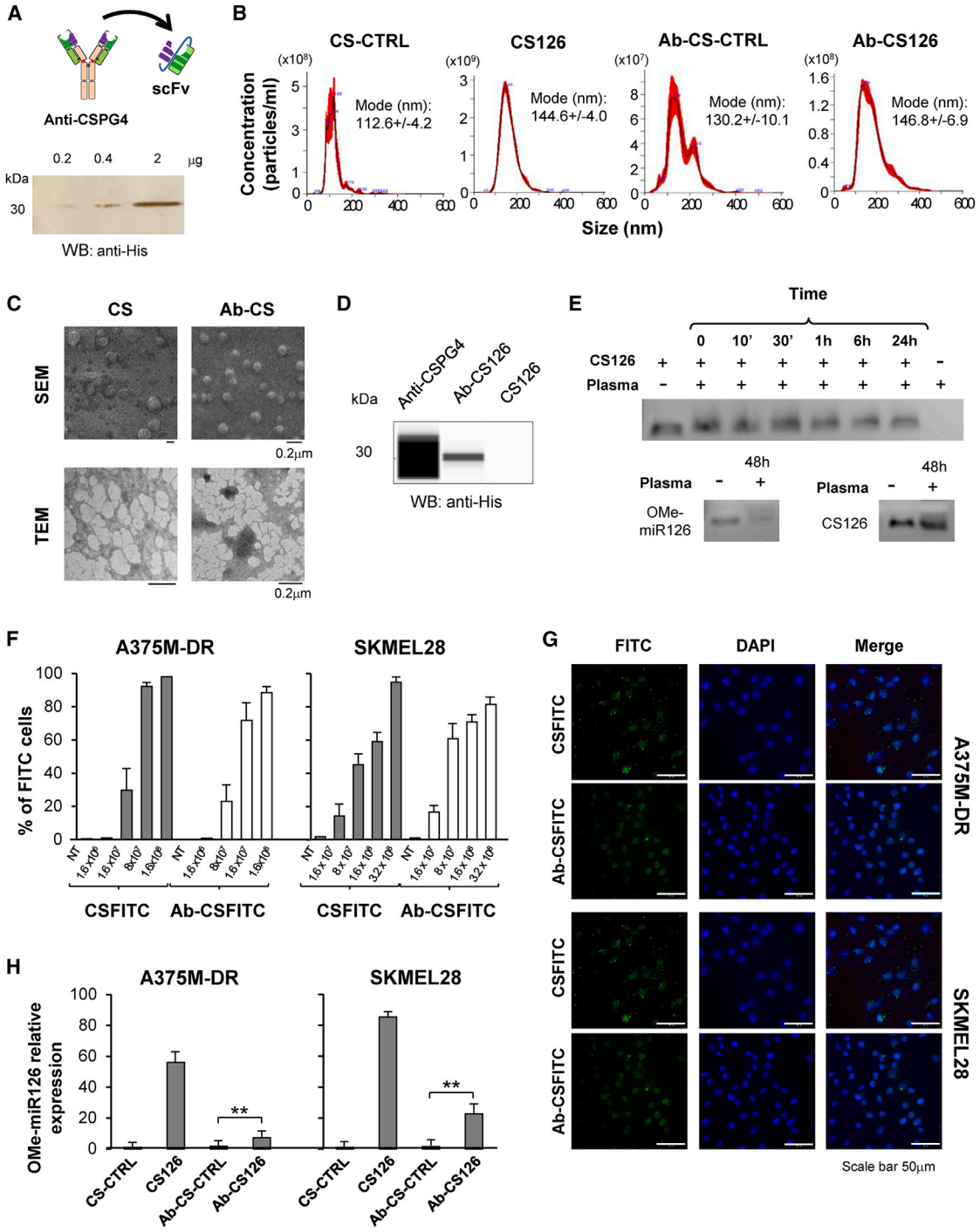

Figure 3. Synthesis and characterization of chitosan NPs

(A) Schematic representation of antibody fragment (scFv) able to bind the specific melanoma marker CSPG4 (scFv-9.2.27) (upper panel) and representative western-blot experiment for antibody quantification (bottom panel). (B) Representative Nanosight characterization of CSs. Concentration (particles/mL) and size (nm) of NPs were reported. (C) Morphology of CS126s and Ab-CS126s analyzed by scanning electron microscopy (SEM) and transmission electron microscopy (TEM). (D) WES analysis of bound anti-CSPG4 protein on Ab-CS126s. Anti-CSPG4 was used as positive control. CS126s were used as negative control. (E) Gel electrophoresis to verify the integrity of the OMe-miR126 sequences entrapped in CS126s cultured with 50% of human plasma. A time course was reported and total integrity was demonstrated until 48 h of

(legend continued on next page)

Quantification of oligos entrapped in CS126s and antibody conjugation to Ab-CS126; stability of CS126 in culture with human plasma

To quantify the amount of oligos (OMe-miR126) entrapped within CS126s, we performed a real-time qRT-PCR. In particular, starting from a fixed number of NPs lysed in acidic water and by interpolation of values obtained with a standard curve, based on amplification of known quantity of OMe-miR126, we were able to evaluate the entrapping efficiency for CS126 and Ab-CS126 of 7428 and 103 OMe-miR126 molecules/NPs, respectively (Figure S2E).

To better characterize our nanocarriers, we evaluated the quantity of bound anti-CSGP4 by WES immunodetection analysis (Figure 3D). A direct comparison with the positive control (soluble anti-CSPG4) allowed us to estimate an amount of 250 pg of anti-CSPG4/6.8×10^7 Ab-CS126s.

As the last step, before performing functional experiments, we evaluated the stability of CS126s in human plasma. Figure 3E shows that the NP-CSs protect OMe-miR126 from degradation for at least 48 h of incubation, as indicated by gel electrophoresis.

In vitro internalization of CS126 and Ab-CS126

To evaluate the internalization efficiency of CS126s and Ab-CS126s, we incubated the melanoma cell lines A375M-DR and SKMEL28 with increasing amounts of both types of fluorescein isothiocyanate (FITC)-labeled NP-CSs. As reported in Figure 3F, flow cytometric analysis showed that, within an hour of incubation of 1.6×10^8 NPs for A375M-DR and 3.2×10^8 for SKMEL28, approximately 100% of the cells in both cases were FITC positive. These results were confirmed by immunofluorescence microscopy (Figure 3G). However, we observed a notable difference between the two types of NPs: despite the comparable percentage of positive cells, Ab-CS126 cells showed a less dispersed distribution, likely due to the direct interaction between the membrane receptor CSPG4 and the anti-CSPG4 antibody conjugated to the NP-CSs. To assess the actual ability to transfer OMe-miR126 within cells, we performed qRT-PCR after incubating cells with an equal number of CS126 and Ab-CS126. We observed an increase of approximately 56-fold and 7.3-fold for CS126 and Ab-CS126, respectively, for A375M-DR and 85-fold and 22.6-fold for CS126 and Ab-CS126, respectively, for SKMEL28 (Figure 3H). This marked difference can be explained by the varying quantity of molecules entrapped in CS126 compared to Ab-CS126 (1.2×10^{-8} and 1.7×10^{-10} pmol/NP, respectively).

Evaluation of CS/Ab-CSs stability and potential toxic effects in mouse model

After evaluating the OMe-miR126 stability in the presence or absence of CS coating (Figure 3E), we tested their kinetics in *in vivo* experiments. To this end, we conjugated CSs and Ab-CSs with FITC (CS-FITCs and Ab-CS-FITCs). The analysis of plasma of mice injected with CS-FITCs and Ab-CS-FITCs revealed a rapid disappearance of fluorescence that was below the limit of detection 60 min post injection (Figure 4A). To evaluate whether the disappearance of the NPs was due to enzymatic degradation in the vascular system or to distribution to other tissue compartments, we incubated CS-FITCs and Ab-CS-FITCs *in vitro* in the presence of 50% plasma. CS-FITCs and Ab-CS-FITCs fluorescent NPs were present until the sixth day of incubation in plasma, with Ab-CS-FITCs showing a higher stability (Figure S3A). We thus analyzed tissues obtained from main organs of mice injected with CS-FITCs or Ab-CS-FITCs by fluorescence microscopy and we found a clear FITC signal in the lung, liver, kidney, and spleen (Figure 4B). To confirm the presence of NPs in mouse tissues, we stained histology slides with an antibody specific for the His-tag of anti-CSPG4, confirming the presence of a signal in the section of kidney (Figure 4C) of the mouse injected with Ab-CS-FITCs.

Before starting *in vivo* treatments, we evaluated the potential toxic effect of CS126s and Ab-CS126s in repeated treatment of mice. We injected a group of mice with intravenous CS126s or Ab-CS126s three times a week for 4 weeks (see section "materials and methods"), and no toxic effect was observed, as indicated by the maintenance of normal weight and health of the treated mice (data not shown).

Effect of CS126 and Ab-CS126 on cell migration

As a final step, before carrying out the *in vivo* experiments, we evaluated the migration capabilities of A375M-DR and SKMEL28-DR cells after exposure to NP-CSs. We observed a decrease in the chemotaxis abilities of CS126s-A375M-DR- and CS126s-SKMEL28-DR-treated cells. Moreover, in agreement with the known relevance of CSPG4 protein for the growth and motility of melanoma cells, we observed a similar decrease of chemotaxis in A375M-DR and SKMEL28-DR treated with Ab-CS-CTRLs, whereas no reduction was observed using CS-CTRL. A more obvious decrease was observed using Ab-CS126s, probably due to the combinatorial effect of OMe-miR126 trapped inside and the antibody on the NPs surface (Figure S3B and data not shown).

In vivo experiments: Strong inhibition of tumor growth and metastatic spread by combined therapy of Ab-CS126 and PIK-75

Our previous experience highlighted the impossibility of obtaining metastases from melanoma cells resistant to treatment with dabrafenib (A375M-DR) by intravenous injection. Thus, we established a reproducible animal model for serial quantification of *in vivo* metastatic tumor burden. With this aim, we injected A375M-DR stably expressing firefly luciferase and GFP (A375M-DR-LUC-GFP) into the spleen of severely immunodeficient mice. To avoid a predominant

incubation. (F) Evaluation of internalization of NPs in A375M-DR and SKMEL28 cell lines by fluorescence-activated cell sorting (FACS) analysis. Cells were incubated with increasing amounts of CS-FITCs and Ab-CS-FITCs for 20 and 60 min, respectively. Data are shown as mean ± SD. (G) Fluorescent microscopy visualization of A375M-DR and SKMEL28 cell lines incubated with CS-FITCs and Ab-CS-FITCs for 1 h. Nuclei of recipient cells were counterstained with Hoechst 33258. (H) qRT-PCR to evaluate the increase of miR126-expression in the A375M-DR and SKMEL28 acceptor cell lines after internalization of the same number of CSs. U6 snRNA was used as normalizer. Data are shown as mean ± SD, **p Value < 0.01.

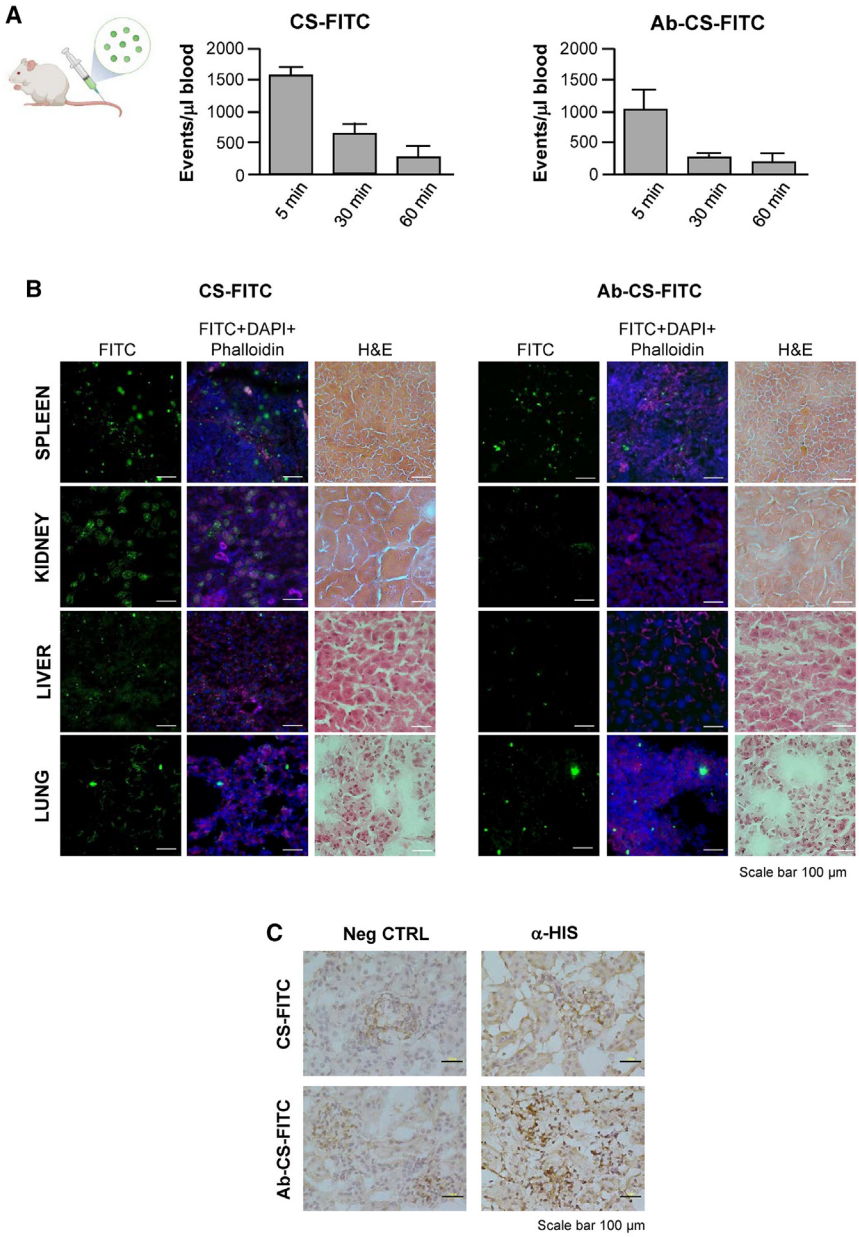

Figure 4. *In vitro* and *in vivo* experiments to evaluate CS-FITCs and Ab-CS-FITCs stability

(A) FACS analysis of retro-orbital collected plasma mice injected with CS-FITCs or Ab-CS-FITCs. Columns represent the mean ± SD. (B) Immunofluorescence microscopy analysis of the main organs of CS-FITCs- and Ab-CS-FITCs-injected mice. (C). Immunostaining of kidney sections using a specific antibody against scFv-9.2.27 in mice injected with CS-FITCs and Ab-CS-FITCs.

growth of tumors in the injection site, splenectomy was performed 30 min after injection. Tumor growth was monitored *in vivo* by bioluminescent imaging IVIS (*in vivo* imaging system) (Figure 5A).

About 2 weeks after inoculation, when the signal was barely detectable, the mice were randomly allocated to six treatment arms. Specifically, (1) control group, (2) PIK-75, (3) Ab-CS126s, (4) PIK-75 + CS126s, (5) PIK-75 + Ab-CS-CTRLs, and (6) PIK-75 + Ab-CS126s. All groups received dabrafenib as reported in section "materials and methods". The specific treatments for each group were initiated in each animal when the region of interest (ROI) measured by IVIS reached approximately 10^4 photons/s/cm^2/sr.

Statistical analysis comparing the slopes of the tumor growth curves in the respective groups highlighted a stronger inhibition in the group treated with PIK-75 + Ab-CS126s compared with other groups (Figure 5B). The mean of IVIS values for each group is reported in Figure S3C.

After the animals were sacrificed, organ analysis confirmed reduced tumor growth in the liver but also a very strong reduction of metastases formation in the lungs. To confirm the greater oncosuppressive efficacy of Ab-CS126 compared to CS126, we performed qRT-PCR on liver samples from three groups: 3,3′diaminobenzidine (DAB), DAB + PIK-75+CS126, and DAB + PIK-75+Ab-CS126 (three animals per group). The expression of human-specific GAPDH (Figure S4A, right panel) aligned with IVIS measurements, indicating a significant reduction in the number of tumor cells in the DAB + PIK-75 + Ab-CS126 group compared to controls (Figure S4A, left panel). The efficiency of miR126 delivered by Ab-CS126 and CS126 was indirectly demonstrated through the evaluation of the miR126 target, human p85-β. This quantification revealed a greater reduction in the expression of human p85-β expression in the DAB + PIK-75 + Ab-CS126 group compared to respective controls (Figure S4B). We used the p85-β target to assess the effectiveness of NPs in delivering miR126 (Figure S4C) due to the inability of qRT-PCR to differentiate between human and murine miR126 and because it testifies to the intracellular activity of the oligo. Figure 5C shows representative images of each group, while the complete panel of all groups is shown in Figures S5 (control), S6 (PIK-75), S7 (Ab-CS126s), S8 (PIK-75 + CS126s), S9 (PIK-75 + Ab-CS-CTRLs), and S10 (PIK-75 + Ab-CS126s). Altogether, these results show that the use of Ab-CS126s in combination with PI3K/AKT inhibitors could be a treatment option for all those patients in whom conventional therapy no longer has any effect. To confirm the effectiveness of the PIK-75 + Ab-CS126s combination, we conducted immunofluorescence experiments using the anti-CSPG4 antibody on lung sections

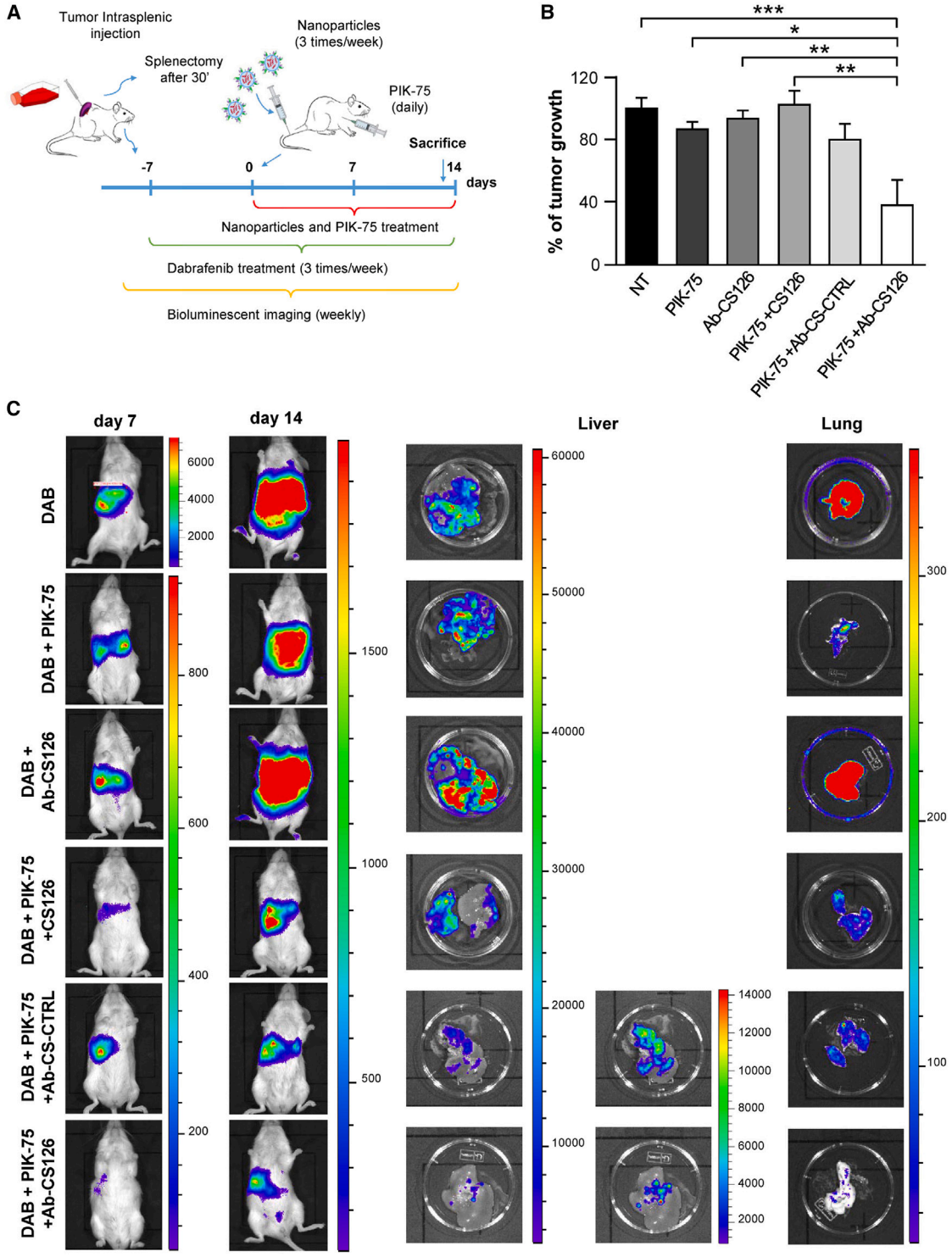

Figure 5. Evaluation of tumor suppressor role played by NPs contained OMe-miR126 in *in vivo* experiments

(A) Schematic animal model. A375M-DR stably expressing firefly luciferase and GFP (A375M-DR-LUC-GFP) were injected into the spleen of severely immunodeficient mice. The splenectomy was performed after 30 min. About 2 weeks after inoculation, when the signal was barely detectable, the mice were randomly allocated to six treatment arms. Tumor engraftment was monitored weekly by *in vivo* bioluminescent imaging. The DAB, PIK-75, and NPs treatments have been administered as indicated. (B)

(legend continued on next page)

of NOD scid gamma (NSG)-treated mice. As shown in Figure 6, a strong positive signal was observed in the sections of the NSG-treated mouse with DAB, while, as expected, a weak signal was detected in the mouse treated with PIK-75 + Ab-CS126s, and no signal was observed in healthy animals and mice treated with the PIK-75 + Ab-CS126s combination but not injected with A375M-DR cells. Taken together, these results confirm the efficacy of the PIK-75 + Ab-CS126 treatment in reducing tumor nodule growth.

DISCUSSION

The results presented in this study represent a further development of the investigation conducted by our group on the oncosuppressive role of miR126 in melanoma, particularly during the metastatic phase of this disease. Before the approval of immune check-point inhibitors, the therapy of advanced-stage BRAF-mutation-positive melanoma relied on the use of BRAF inhibitors and, more recently, on the combined inhibition of BRAF and MEK.[4] Even with the double blockade of the MAPK pathway, disease progresses in most patients after some months. Immune check-point inhibitors, even if they seem to cause a lower reduction of the tumor mass in the first time points, produce a more prolonged response in a relevant percentage of patients. Recent studies have highlighted that the administration of programmed cell death protein 1 (PD-1) and cytotoxic T lymphocyte-associated protein 4 (CTLA-4) inhibitors until disease progression, followed by MAPK inhibition, yields a better response compared to the reverse administration.[41] Other authors have observed a similar behavior; however, they showed that a short course of encorafenib plus binetimib followed by ipilimumab plus nivolumab until progression and then encorafenib plus binetimib produces a better outcome in OS mainly by reducing the lower survival with immune check-point inhibitors in the first months.[42,43] The availability of these two therapeutic strategies allows prolonged survival in a large percentage of patients with advanced BRAF-mutated melanoma; however, a significant proportion of patients still die of the disease during the years after diagnosis. Patients with relapse after these two steps of treatment would need agents targeting different mechanisms of tumor viability.

Here, we show that *in vitro* miR126 synergizes with PI3K inhibitor (PIK-75) in reducing the proliferation of BRAF-mutated melanoma cells either resistant or sensitive to BRAF inhibition. We observed a strong inhibition of liver and lung metastases. This inhibitory effect is achieved when miR126 is co-administered with a PI3K/AKT pathway inhibitor (PIK-75), as predicted by the *in vitro* experiments conducted on two different metastatic melanoma cell lines (A375M and SKMEL28) and their dabrafenib-resistant counterparts (A375M-DR and SKMEL28-DR). Previous studies have shown that one of the multiple proteins targeted by miR126 is p85-β, which transduces downstream signals of the PI3K pathway, leading to AKT phosphorylation, through the formation of a dimer with the p110α subunit, a target of PIK-75. The convergence of the two inhibitors (miR126 and PIK-75) on targets belonging to the same pathway explains the observed synergistic effect in inhibiting tumor cell growth in the combined treatment.[17] An important aspect to consider is the crosstalk between the PI3K/AKT and MAPK/ERK pathways in tumor cells, with MAPK/ERK being constitutively active in approximately 60% of melanomas carrying the BRAF V600E mutation. When targeted therapy inhibits the MAPK/ERK pathway, the hyper-activation of the PI3K/AKT pathway can compensate the inhibition of the other pathway. The molecular mechanisms underlying the development of resistance are multiple.[14] However, we have observed that simultaneous treatment of melanoma cells with inhibitors of the PI3K/AKT (miR126 and PIK-75) and MAPK/ERK (vemurafenib or dabrafenib) pathways results in a synergistic inhibitory effect. Furthermore, what is more interesting is that, even after the development of resistance to dabrafenib or vemurafenib, treatment with miR126 and PIK-75 remains effective. These findings prompted us to search for a way to deliver miR126 *in vivo* efficiently also by protecting it from enzyme degradation in the plasma. We first chemically modified the canonical sequence of miR126, increasing its stability in plasma (OMe-miR126) (Figure 1A). After confirming that this sequence retained all the previously demonstrated properties of its normal counterpart, we developed a nanocarrier capable of efficiently encapsulating the sequence. Tumor tissues lack the vasculature-supporting environment, which leads to the formation of loose vessels that allow for increased NP accumulation in tumors.[44] NP-CSs, which show good biocompatibility, biodegradability, and low toxicity, have been shown to localize near tumors by taking advantage of the enhanced permeability and retention (EPR) of tumor tissues. However, this passive targeting is not specific to tumor cells. Combining active and passive targeting strategies can enhance drug delivery to tumor cells, such as by functionalizing NPs with ligands that target tumor-specific receptors. The positively charged NP-CSs can electrostatically interact with the negatively charged miR molecules, protecting them from degradation and facilitating their uptake by cancer cells. Furthermore, NP-CSs can be easily functionalized by targeting ligands to improve their specificity toward cancer cells.[45] In our study, we synthesized NP-CSs loaded with OMe-miR126 or its corresponding control sequence (CS126s and CS-CTRLs respectively), which were subsequently functionalized by conjugating them to the variable domain of an antibody that recognizes the tumor marker CSGP4.

Before proceeding to *in vivo* studies, the NPs were fully characterized in terms of their size, ζ potential, oligonucleotide quantity entrapped, antibody conjugation efficiency, and *in vitro* delivery capacity. To track the kinetics of the NP-CSs and antibody-conjugated NP-CSs in a murine model, we made them traceable using FITC. In approximately 1 h, we observed the disappearance of CS-FITC and Ab-CS-FITC from the blood and their accumulation in the liver and

Comparison of the slopes of the growth curves in each group of treatments. Data are shown as mean ± SD of angular coefficients of growth curves obtained by plotting ROI measurements at different time for each mouse of each group. *p Value < 0.05, **p value < 0.01, and ***p value < 0.001. (C) Fluorescent IVIS images of one representative mouse of six treatment arms at 7 and 14 days after the start of treatments. In particular, untreated group (NT), PIK-75; Ab-CS126s; PIK-75 + CS-126s; PIK-75 + Ab-CSs; PIK-75 + Ab-CS126s. All groups received dabrafenib according to the protocol reported in section "materials and methods". In the right panel, liver and lung from each mouse were imaged individually in the IVIS spectrum.

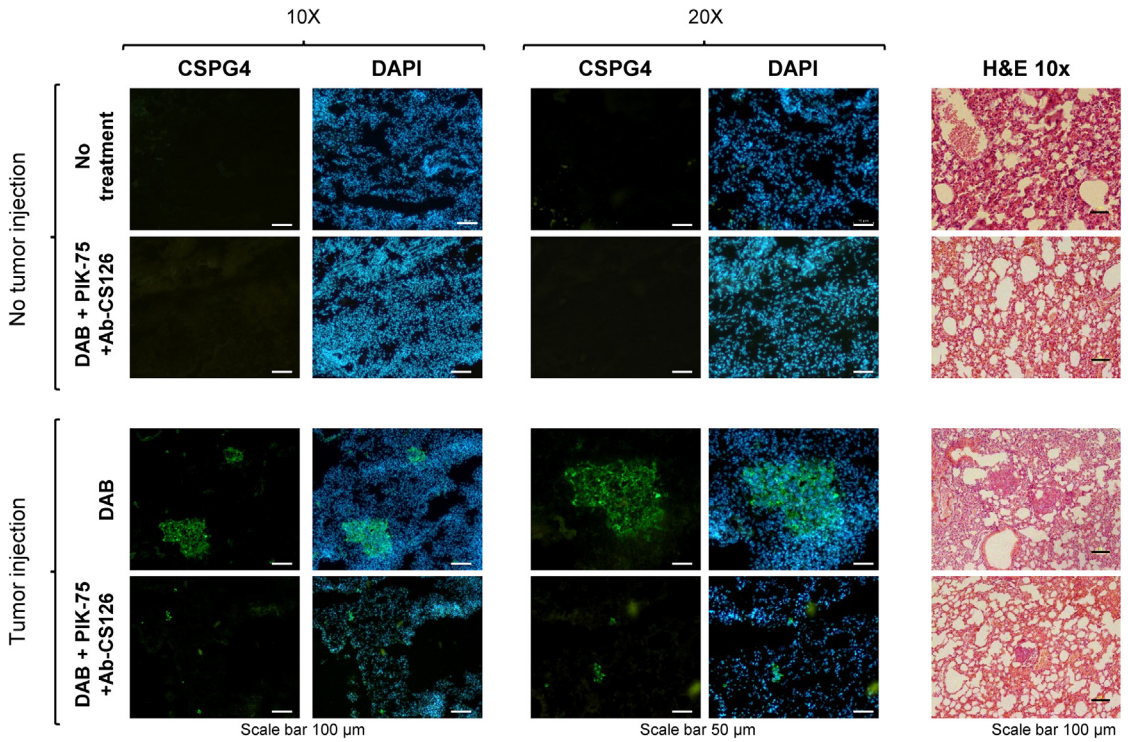

Figure 6. Immunofluorescence analysis of lung sections of NSG-treated mice

Immunofluorescence of mice cryopreserved lung sections. Labeling was performed using the anti-CSPG4 mAb and goat anti-mouse IgG secondary antibody Alexa Fluor 488 (green). Nuclei were counterstained with DAPI. Scale bars, respectively, 100 µm (10× original magnification) and 50 µm (20× original magnification). The last column shows H&E morphology of paraffin-embedded lung tissue sections of the same treated mice. Scale bar, 100 µm (original magnification 10×).

lungs, two of the main target organs of metastatic melanoma, with no observed toxic effects on the treated animals. NSG mice injected with A375M-DR and treated with Ab-CS126 and PIK-75 showed a significant reduction in tumor growth compared to all control groups.

This result not only confirmed the synergy between miR126 and PIK-75 in the treatment of metastatic melanoma resistant to MAPK inhibitors but also demonstrated that targeting CSPG4 is a promising strategy to treat melanoma. We paid careful attention to the size and ζ potential of the NPs, the quantity of entrapped oligonucleotides, and the efficiency of conjugation to the antibody. These technical controls ensured the reproducibility of our results and minimized any potential variability that could have affected the outcomes. While our study provides promising results, there are still several important aspects that require further investigation before the treatment can be applied in clinical settings. For example, the long-term toxicity of the proposed treatment needs to be thoroughly evaluated to ensure its safety and effectiveness over prolonged periods of time. Nevertheless, the data presented in our study demonstrate the importance of combining miR126 and PI3K/AKT inhibitors in the treatment of melanoma that has developed resistance to MAPK inhibitors. Furthermore, our results suggest that the nanocarrier we synthesized and functionalized with a tumor-specific antibody could serve as a promising tool for delivering miR126 to the tumor in a targeted manner. The findings from this study hold promising implications for potentially expanding the application of this system to cancer types where treatment with oncosuppressive miRs could represent a significant therapeutic breakthrough.

MATERIALS AND METHODS

Cell culture and transfection

The malignant human melanoma cell line A375M was kindly provided by R. Giavazzi (Istituto Mario Negri, Bergamo, Italy). The human melanoma cell line SKMEL28 was obtained from S. D'Atri (IDI IRCCS, Rome, Italy). Vemurafenib-resistant A375M (A375M-VR), dabrafenib-resistant A375M (A375M-DR), and dabrafenib-resistant SKMEL28 (SKMEL28-DR) cell lines were generated by culturing parental cells in increasing concentrations of vemurafenib or dabrafenib (from 0.5 to 10 µM; Selleckchem, Munich, Germany) for at least 2 months and subsequently maintained in full growth medium containing 5 µM vemurafenib for A375M-VR or 1.5 µM dabrafenib for A375M-DR and SKMEL28-DR. All melanoma cell lines were cultured in Dulbecco's modified Eagle's medium (Euroclone, Milan, Italy) supplemented with 10% fetal bovine serum (FBS) (Euroclone). Cells were incubated at 37°C with 5% CO_2 in a humidified chamber. Cell lines were authenticated by standard short tandem repeat-based

genotyping (Department of Oncology and Molecular Oncology, ISS, Rome, Italy).

Selected sequences (Table S1) were transfected using Lipofectamine 2000 (Invitrogen by Thermo Fisher Scientific) according to the manufacturer's instructions.

CellTiter-GLO

For the proliferation assay, we measured ATP levels using CellTiter-Glo (Promega Corporation, Madison, WI, USA) according to the manufacturer's instructions and quantified using an MultiLabel Plate Reader VICTOR X3 (PerkinElmer, Norwalk, CT, USA).

RNA extraction and real-time qRT-PCR

Total RNA was extracted with Total RNA Purification micro kit (Norgen BIOTEK, Thorold, ON, Canada) according to the manufacturer's specifications. Then 50 ng of RNA were reverse transcribed by TaqMan MicroRNA Reverse Transcription Kit (Applied Biosystems by Thermo Fisher Scientific; 4366596). To detect the expression levels of miR-126-3p (assay ID 002228; Thermo Fisher Scientific), human p85-β (assay ID Hs01550149_m1; Thermo Fisher) and human GAPDH (assay ID Hs99999905_m1) real-time PCR were carried out using SensiFAST Probe Hi-ROX kit (Bioline, Memphis, TN, USA; BIO-82020). Normalization was performed by using U6 small nuclear RNA (snRNA) (assay ID 001973; Thermo Fisher Scientific) and 18S rRNA (assay ID 4319413E; Thermo Fisher).

Automated capillary western immunoassay

Total cell lysates were prepared by using Nonidet-P40 lysate buffer as previously reported.[17] Analysis of protein expression was performed using automated capillary western immunoassay (WES) technology by ProteinSimple according to the manufacturer's protocol (Bio-Techne, Minneapolis, MN, USA). Compass software (ProteinSimple) was used to acquire and analyze the data and generate gel images and chemiluminescence intensities. The primary antibodies p85-β (1:50, ab28356, Abcam, Cambridge, UK), histidine-tag (clone AD1.1.10) (1:50, MCA1396GA; Bio-Rad), and β-actin (1:100, A5441; Sigma-Aldrich, St. Louis, MO, USA) were used with anti-mouse (DM-002) secondary antibody provided by ProteinSimple.

Synthesis of antibodies

The gene sequences of the VH and VL of the anti-CSPG4 9.2.27 murine mAb were used to design a scFv. The VH and the VL were linked by a peptide of 15 amino acids, and tag FLAG and tag 6 histidine (6 His) sequences were also added. The anti-CSPG4 scFv construct into phagemid vector was obtained as a synthesis product from GenScript (Rijswijk, Netherlands). HB2151 *Escherichia coli* (K12, ara D(lac-pro), thi/F'proA + B+, lacIqZ DM15) cells were electroporated with the recombinant phagemids.

Soluble scFv purification

Soluble scFv purification was performed as described by Flego et al.[37] Electroporated HB2151 *E. coli* expressing the anti-CSPG4 scFvs were cultured at 37°C in 2xTY (Sigma-Aldrich by Merck) containing 100 μg/mL ampicillin and 0.1% glucose up to optical density 600 nm (OD_{600}) 0.5. The expression of scFvs was induced by adding IPTG (isopropyl β-D-thiogalactopyranoside) 1 mM to the culture. The bacterial culture was incubated overnight at 30°C. After the incubation, it was centrifuged and the scFv-containing supernatant was collected. ScFv antibodies were precipitated with ammonium sulfate and dialyzed in PBS. His-tagged scFv antibodies were purified by immobilized metal affinity chromatography using Ni^{2+}-nitriloacetic acid agarose (Ni-NTA resin, 1018244, Qiagen, Milan, Italy). ScFv fragments were eluted with 250 mM imidazole in PBS, dialyzed, quantified by UV absorbance at 280 nm, tested for specific antigen recognition on A375M-DR melanoma and 293FT cells by fluorescence-activated cell sorting (FACS) analysis, and stored at −80°C.

CSPG4 detection on cell surface

The ability of anti-CSPG4 scFvs to bind CSPG4 expressed on cell surface was evaluated by flow cytometry analysis. About 2.5×10^5 A375M-DR melanoma and 293FT cells were resuspended in 200 μL of PBS containing 25 μg/mL of purified scFv antibody and incubated for 1 h at room temperature (RT). After washing, cells were resuspended for 30 min at 4°C in PBS containing 10 μg/mL anti-6×His antibody AD1.1.10 (MCA1396GA Bio-Rad) and, after washing, cells were incubated with 6 μg/mL of FITC-goat anti-mouse immunoglobulin (Ig) G (31569, Thermo Fisher Scientific) for 30 min at 4°C. The irrelevant scFv anti-GO (Ascione at al., 2004) was used as negative control. After staining, the cell samples were washed, maintained at 4°C, and immediately analyzed by CytoFLEX LX Flow Cytometer, UV-Violet-Blue-Yellow Green-Red (U-V-B-Y-R) Series, Beckman Coulter. Data were analyzed with Kaluza Analysis Software (Beckman Coulter, Milan, Italy).

ELISA

Coating was with 0.5 mg of antigen in PBS in 96-well ELISA plates (Nunc MaxiSorp) overnight at RT. The following day, a blocking solution consisting of 2% non-fat dry milk in PBS (MPBS) was added and plates incubated for 2 h; plates were then washed with PBS/0.05% Tween 20 (TPBS) and incubated for 2 h at RT with 50 mL of supernatants containing soluble scFv CSPG4 antibody, anti-FLAG antibody (1.6 mg/mL, Sigma-Aldrich by Merk Life Science, Milan, Italy) and anti-mouse HRP-conjugated antibody (1.6 mg/mL Dako; Denmark). The reaction was developed using 3,31-5,51-tetramethylbenzidin BM blue, POD substrate, soluble (Roche Diagnostics, Indianapolis, IN, USA), and stopped by adding 50μL of 1 M sulfidric acid. The reaction was detected with an ELISA reader (Bio-Rad), and the results were expressed as A (absorbance) = A (450 nm) − A (620 nm).

Preparation of NP-CSs entrapping OMe-miR126 or OMe-CTRL

NP-CSs entrapping OMe-miR126 (CS126s) and NP-CSs entrapping OMe-CTRL (CS-CTRLs) were prepared by ionotropic gelation, a

polyelectrolyte complexation method, mixing two solutions of oppositely charged polymers, in a 1:1 v/v ratio.

A 1-mg/mL chitosan solution was prepared in 0.1 M aqueous acetic acid solution (pH = 4). Then, 80 μg of oligonucleotide were diluted with an appropriate volume of sterile double-distilled water to obtain an N/P ratio of 10. The nucleic acid was added to 500 μL of the chitosan solution under magnetic stirring. The mixture was stirred for 15 min, left at RT for 30 min to allow the spontaneous formation of CS126s, and then stored for 24 h at 4°C before use.

Entrapment efficiency of loaded nucleic acid

The amount of unbound nucleic acid was determined by a UV-visible spectrophotometer. Samples were centrifuged at 14,000 rpm at 4°C for 30 min to facilitate the precipitation of polyplexes, and supernatants were analyzed spectrophotometrically. An entrapment efficiency of 70% ± 9.3% was achieved according to the following formula:

$$E\% = (Ai - Af) / Ai \times 100$$

where Ai is the initial amount of nucleic acid added to the solution (μg) and Af is the final amount of nucleic acid in the supernatant (μg).

Conjugation of CS126s and CS-CTRLs with antibody fragment

1-Ethyl-3-(3-dimethylaminopropyl) carbodiimide (EDC)/ N-hydroxysuccinimide (NHS) chemistry was used to conjugate CS126s and CS-CTRLs with the antibody fragment (Figure 4A), and 500 μg of NPs were precipitated by centrifugation (14,000 rpm, 30 min, 4°C). The pellet was suspended in 500 μL of PBS. Subsequently, 50 μg of antibody were diluted in an equal volume of MES buffer (pH = 6). EDC and NHS at a 2:5 molar ratio were added to the reaction mixture and kept under magnetic stirring for 15 min. After adjusting the pH to 7, the NP solution was added, incubating the reaction mixture at RT for 2 h under magnetic stirring. The solution was then transferred into a dialysis membrane and placed in a beaker containing sterile distilled water. Dialysis was allowed for 5 days. The amount of bound antibody was evaluated by means of spectrophotometric measurements.

Nanosight

The number and size of NPs were directly tracked using the Nanosight NS300 system (Nanosight technology, Malvern, UK), configured with a 488-nm laser and a high-sensitivity scientific complementary metal-oxide semiconductor (sCMOS) camera. Videos were collected and analyzed using the NTA software (version 3.0). For each sample, multiple videos of 60-s duration were recorded, generating replicate histograms that were averaged.

SEM analysis

SEM analysis was used to study NP morphology. Samples were deposited on 12-mm-diameter glass coverslips for 30 min and then they were gold coated by sputtering (SCD 040 Balzers device, Bal-Tec). Samples were then examined with a scanning electron microscope (FEI Quanta Inspect FEG; FEI Company, Eindhoven, the Netherlands).

TEM analysis

TEM analysis was used to study NP morphology. A drop of NP suspension was placed onto a formvar-carbon-coated grid. After 2 min, the excess liquid was blotted off with filter paper. Then grids were negative stained with a drop of 1% phosphotungstic acid (PTA) solution. After 1 min, the excess was blotted off with filter paper and the grid allowed to air dry. Samples were examined with a Philips 208 transmission electron microscope (FEI Company, Eindhoven, the Netherlands) operating at 80 kV. Image analysis was carried out by a digital image analyzer analySIS 3.0 (SIS, Germany).

Gel electrophoresis

In order to evaluate the possible adsorption of the nucleic acid on surface and NP stability, samples were examined by gel electrophoresis. Nucleic acids, negatively charged by the presence of phosphate groups, were subjected to an electric field and placed on a 1% agarose gel. CS126s in aqueous solution were loaded on pre-formed gels inside wells and stained with ethidium bromide to observe the DNA rush under UV light.

In vitro experiment: Cells treated with CS-FITCs and Ab-CS-FITCs

A375M or SKMEL28 melanoma cells were seeded in 24-well plates (2×10^5 cells/well) and grown for 24 h. Then, the cells were incubated with different quantities of FITC-conjugated NPs in medium without FBS for 60 min. After treatment, cells were collected and analyzed.

Preparation of frozen tissue sections

After an intraoperative sampling of mouse liver, spleen, kidney, and lung tissues, the frozen sections were included in OCT (05–9801 Bio-Optica, MI-It) and cut on a cryostat (Thermo Scientific Shandon FS, Thermo Fisher Scientific) at −25°C, mounted on coverslips with at least 20 slides per lesion, and cryoconserved in −80°C until the fixation process. Two frozen sections were routinely stained with Mayer's Hematoxylin Solution (MHS-32 Sigma-Aldrich) and Eosin Y solution (SHBN7854 Sigma-Aldrich) and then observed under the microscope for morphology.

Preparation of paraffin-embedded tissue sections

After intraoperative sampling, mouse liver, spleen, kidney, and lung tissues were fixed in 4% formalin for 24–48 h, dehydrated, cleared with VTP300, and embedded in paraffin with BEC150 Bio-Optica (MI-It). Blocks were cut in 2- to 5-μm sections with a microtome (Leica Reichert:Jung 2030, IL60010US), deparaffinized, stained with H&E, and then observed under the microscope for morphology (Nikon Eclipse Ni equipped with DS-Fi2 camera at 10× and 20× magnification).

Immunohistochemical staining

Immunohistochemistry was performed on mouse cryopreserved kidney tissue sections to determine NP localization. Slides were fixed in

4% paraformaldehyde for 10 min, rinsed in PBS, and permeabilized in 0.1% Triton X-100 for 2 min at RT. Tissues were then incubated with murine serum and anti-HIS for the controls and treated tissue, respectively. Samples were stained using Cell and Tissue Staining Kit HRP DAB (R&D System by Bio-Techne). According to the instruction manual, detection is based on the formation of the avidin-biotin complex (ABC) with primary antibody that reacts with tissue antigens under study. Visualization is based on enzymatic conversion of a chromogenic substrate DAB into a brown precipitate by HRP at the sites of antigen localization. Slides were evaluated by using a bright-field Zeiss Axioscope 5 Microscope 10×, 20×, and 40× magnification objectives (Zeiss, Oberkochen, Germany) equipped with Axiocam 305 color.

Immunofluorescence staining

A375M melanoma cells were seeded on 12-mm-diameter coverslips in 24-well plates (1.2×10^4 cells/well) and grown for 24 h. They were incubated with CS-FITCs or Ab-CS-FITCs for 20 min. For immunofluorescence localization studies, slides were fixed in 4% paraformaldehyde for 10 min, rinsed in PBS, and permeabilized in 0.1% Triton X-100 for 2 min at RT. Cells were then incubated with Phalloidin Alexa Fluor 647 nm (PP-10057, Immunological Sciences, Rome, Italy) for 30 min washed and subsequently incubated with DAPI (D1306 Invitrogen by Thermo Fisher Scientific) for 20 min RT in the dark. For CSPG4 immunostaining, slides were washed with 1× PBS and the tissues were blocked and permeabilized in blocking buffer (1× PBS containing 1% bovine serum albumin) for 1 h at RT. Tissues were incubated for 1 h at RT with anti-CSPG4 antibody 9.2.27 (MAB 2029, Millipore, MA, US) diluted 1:500 in blocking buffer, washed three times with 1× PBS, and incubated for 1 h at RT with goat anti-mouse secondary IgG antibodies Alexa Fluor 488, diluted 1:500 in blocking buffer (IS-20010, Immunological Sciences). Finally, cell nuclei were counterstained with DAPI (1:10,000). Slides were mounted with SlowFade anti-fade reagent (Molecular Probes) and evaluated by using a wide-field fluorescence microscope (Zeiss Axioscope 5 Microscope 10×, 20× magnification).

Wound-healing assay

A375M-DR and SKMEL28-DR cells were seeded into 24-well plates and grown to 90% confluence. A linear wound was created in the confluent monolayer by using a 200-μL micropipette tip followed by washing with PBS to remove the cell debris. The cells with 0.5 mL of culture medium (without FBS) were then exposed to NPs. After 48-h incubation, the furrow was photographed and monitored with the JuLI Smart fluorescent cell analyzer microscope (Digital Bio, Waltham, MA, USA) and the empty area of the collected images was quantified by using AlphaViewJ software (ProteinSimple by Bio-Techne).

In vitro stability of CS-FITC and Ab-CS-FITC

With regard to *in vitro* experiment stability, an equal amount of CS-FITCs and Ab-CS-FITCs were incubated at 37°C in murine serum at predetermined time points (T0, 24 h, and 2, 3, and 6 days). At each time point, the serum samples were collected and stored at −20°C.

Samples were analyzed by CytoFLEX LX Flow Cytometer, UV-Violet-Blue-Yellow Green-Red (U-V-B-Y-R) Series (Beckman Coulter) for the presence of CS-FITC and Ab-CS-FITC. Data were analyzed with Kaluza Analysis Software (Beckman Coulter).

In vivo stability of CS-FITC and Ab-CS-FITC

CS-FITC and Ab-CS-FITC were sonicated and injected in female C57/Bl/6 mice, intravenously. At each predetermined time point (5 min, 15 min, 30 min, 1 h), retro-orbital sampling was performed and the samples were stored at −20°C. Samples were analyzed by CytoFLEX LX Flow Cytometer, UV-Violet-Blue-Yellow Green-Red (U-V-B-Y-R) Series (Beckman Coulter) for the presence of CS-FITC and Ab-CS-FITC. Data were analyzed with Kaluza Analysis Software (Beckman Coulter).

In vivo mouse model

A375M-DR-LucGFP cells, transduced with a retroviral vector expressing the firefly luciferase gene (LUC-GFP),[46] were directly injected into the spleen of 8-week-old female NSG nude mice (minimum n = 5 mice per group; Charles River, Wilmington, MA, USA) at a dose of 5×10^4 cells in 200 μL of PBS. Splenectomy was performed 30 min after inoculation, sufficient time for the cells to spread into the hepatic circulation. Assessment of metastatic development was performed by bioluminescence of inoculated cells once a week using the IVIS (PerkinElmer) optical imaging system.

About 2 weeks after inoculation, when the signal was barely detectable, defined by ROI value, the mice were randomly allocated to six treatment arms: a control group (dabrafenib 1.25 μg/g mouse); a group treated with dabrafenib and PIK-75 (2 μg/g mouse) in combination; the third mice group treated with dabrafenib and the Ab-CS126s; the fourth group treated with dabrafenib, PIK-75, and CS126s; the fifth group treated with dabrafenib, PIK-75, and Ab-CSC(−); and the last group with the combination of drugs and the Ab-CS126s. Dabrafenib was administered three times weekly and PIK-75 daily, both intraperitoneally. Ab-CS126s were administered three times week intravenously. Animal experiments were performed at the Istituto Superiore di Sanità (Rome, Italy) according to Italian law and institutional guidelines (authorization n.126/2021-PR, Protocol D9997.122).

Statistical analysis

Unless indicated otherwise, all data are presented as mean + standard deviation (SD) and results are representative of at least three independent experiments. Statistical analysis was performed using Student's t test and ANOVA, and significance is indicated in plots using asterisks as follows: *$p < 0.05$, **$p < 0.01$, and ***$p < 0.001$.

The EOB independence model was used to quantify the synergy for each compound pair. EOB evaluates the difference between

the observed and expected inhibition of different drug dose combinations.

Statistical analysis was performed by means of GraphPad prism v4.0 (GraphPad Software, La Jolla, CA, USA, www.graphpad.com).

Kaplan-Meier survival curves were plotted and differences in survival between groups of patients were compared using the log rank test.

DATA AND CODE AVAILABILITY

The data that support the findings of this study are available from the authors on request.

SUPPLEMENTAL INFORMATION

Supplemental information can be found online at https://doi.org/10.1016/j.ymthe.2023.11.021.

ACKNOWLEDGMENTS

This research and Maria Beatrice Arasi fellowship were supported by Regione Lazio, Progetto di Gruppo di Ricerca (Prot.15263), principal investigator M.B., and MAECI–MINISTERO DELLA SALUTE, Progetti di Grande Rilevanza, L. 401/90 (PGR01243), principal investigator N.F. We would like to thank A. Giuliani for statistical analysis and critical reading of the manuscript and A. Calcabrini for supporting TEM/SEM analyses and proofreading.

AUTHOR CONTRIBUTIONS

M.B.A., *in vitro* and *in vivo* experiments, data analysis, and manuscript writing support; G.D.L. and M.S., *in vivo* experiments; L.C., M.C.P., and C.P., synthesis of nanocarriers; F.P., *in vitro* experiments and support for manuscript graphic section; M.F., synthesis of anti-CSPG4; E.P., immunohistochemical and immunofluorescence experiments; A.S. and M.C., TEM and SEM analysis; L.P., FACS analysis; V.L., OS analysis; G.A.C., M.B., and C.P., critical supervision and support for the final version of the manuscript; and F.F. and N.F., study conception and design, data analysis, and manuscript writing.

DECLARATION OF INTERESTS

The authors declare that the data presented in this study are the subject of an industrial invention patent field on behalf of the Istituto Superiore di Sanità.

REFERENCES

1. Situm, M., Buljan, M., Kolić, M., and Vučić, M. (2014). Melanoma—clinical, dermatoscopical, and histopathological morphological characteristics. Acta Dermatovenerol. Croat. *22*, 1–12.
2. Saginala, K., Barsouk, A., Aluru, J.S., Rawla, P., and Barsouk, A. (2021). Epidemiology of Melanoma. Med. Sci. *9*, 63.
3. Bolick, N.L., and Geller, A.C. (2021). Epidemiology of Melanoma. Hematol. Oncol. Clin. North Am. *35*, 57–72.
4. Guo, W., Wang, H., and Li, C. (2021). Signal pathways of melanoma and targeted therapy. Signal Transduct. Target. Ther. *6*, 424.
5. Davies, H., Bignell, G.R., Cox, C., Stephens, P., Edkins, S., Clegg, S., Teague, J., Woffendin, H., Garnett, M.J., Bottomley, W., et al. (2002). Mutations of the BRAF gene in human cancer. Nature *417*, 949–954.
6. Ostrowski, S.M., and Fisher, D.E. (2021). Biology of Melanoma. Hematol. Oncol. Clin. North Am. *35*, 29–56.
7. Wellbrock, C., and Arozarena, I. (2016). The Complexity of the ERK/MAP-Kinase Pathway and the Treatment of Melanoma Skin Cancer. Front. Cell Dev. Biol. *4*, 33.
8. Namikawa, K., and Yamazaki, N. (2019). Targeted Therapy and Immunotherapy for Melanoma in Japan. Curr. Treat. Options Oncol. *20*, 7.
9. Luke, J.J., Flaherty, K.T., Ribas, A., and Long, G.V. (2017). Targeted agents and immunotherapies: optimizing outcomes in melanoma. Nat. Rev. Clin. Oncol. *14*, 463–482.
10. Davis, L.E., Shalin, S.C., and Tackett, A.J. (2019). Current state of melanoma diagnosis and treatment. Cancer Biol. Ther. *20*, 1366–1379.
11. Corcoran, R.B., Settleman, J., and Engelman, J.A. (2011). Potential therapeutic strategies to overcome acquired resistance to BRAF or MEK inhibitors in BRAF mutant cancers. Oncotarget *2*, 336–346.
12. Song, C., Piva, M., Sun, L., Hong, A., Moriceau, G., Kong, X., Zhang, H., Lomeli, S., Qian, J., Yu, C.C., et al. (2017). Recurrent Tumor Cell-Intrinsic and -Extrinsic Alterations during MAPKi-Induced Melanoma Regression and Early Adaptation. Cancer Discov. *7*, 1248–1265.
13. Long, G.V., Fung, C., Menzies, A.M., Pupo, G.M., Carlino, M.S., Hyman, J., Shahheydari, H., Tembe, V., Thompson, J.F., Saw, R.P., et al. (2014). Increased MAPK reactivation in early resistance to dabrafenib/trametinib combination therapy of BRAF-mutant metastatic melanoma. Nat. Commun. *5*, 5694.
14. Luke, J.J., and Schwartz, G.K. (2013). Chemotherapy in the management of advanced cutaneous malignant melanoma. Clin. Dermatol. *31*, 290–297.
15. Varrone, F., and Caputo, E. (2020). The miRNAs Role in Melanoma and in Its Resistance to Therapy. Int. J. Mol. Sci. *21*, 878.
16. Lin, N., Zhou, Y., Lian, X., and Tu, Y. (2015). Down-regulation of tissue microRNA-126 was associated with poor prognosis in patients with cutaneous melanoma. Int. J. Clin. Exp. Med. *8*, 4297–4301.
17. Pedini, F., De Luca, G., Felicetti, F., Puglisi, R., Boe, A., Arasi, M.B., Fratini, F., Mattia, G., Spada, M., Caporali, S., et al. (2019). Joint action of miR-126 and MAPK/PI3K inhibitors against metastatic melanoma. Mol. Oncol. *13*, 1836–1854.
18. Lu, M., Xing, H., Zheng, A., Huang, Y., and Liang, X.J. (2023). Overcoming Pharmaceutical Bottlenecks for Nucleic Acid Drug Development. Acc. Chem. Res. *56*, 224–236.
19. Arasi, M.B., Pedini, F., Valentini, S., Felli, N., and Felicetti, F. (2020). Advances in Natural or Synthetic Nanoparticles for Metastatic Melanoma Therapy and Diagnosis. Cancers (Basel) *12*, 2893.
20. Ahmed, T.A., and Aljaeid, B.M. (2016). Preparation, characterization, and potential application of chitosan, chitosan derivatives, and chitosan metal nanoparticles in pharmaceutical drug delivery. Drug Des. Devel. Ther. *10*, 483–507.
21. Zhao, Y., Zhang, Z., Pan, Z., and Liu, Y. (2021). Advanced bioactive nanomaterials for biomedical applications. Exploration (Beijing) *1*, 20210089.
22. Cosco, D., Cilurzo, F., Maiuolo, J., Federico, C., Di Martino, M.T., Cristiano, M.C., Tassone, P., Fresta, M., and Paolino, D. (2015). Delivery of miR-34a by chitosan/PLGA nanoplexes for the anticancer treatment of multiple myeloma. Sci. Rep. *5*, 17579.
23. Dahlman, J.E., Barnes, C., Khan, O., Thiriot, A., Jhunjunwala, S., Shaw, T.E., Xing, Y., Sager, H.B., Sahay, G., Speciner, L., et al. (2014). In vivo endothelial siRNA delivery using polymeric nanoparticles with low molecular weight. Nat. Nanotechnol. *9*, 648–655.
24. Ilieva, K.M., Cheung, A., Mele, S., Chiaruttini, G., Crescioli, S., Griffin, M., Nakamura, M., Spicer, J.F., Tsoka, S., Lacy, K.E., et al. (2017). Chondroitin Sulfate Proteoglycan 4 and Its Potential As an Antibody Immunotherapy Target across Different Tumor Types. Front. Immunol. *8*, 1911.
25. Felli, N., Errico, M.C., Pedini, F., Petrini, M., Puglisi, R., Bellenghi, M., Boe, A., Felicetti, F., Mattia, G., De Feo, A., et al. (2016). AP2 alpha controls the dynamic balance between miR-126&126*and miR-221&222 during melanoma progression. Oncogene *35*, 3016–3026.
26. Felli, N., Felicetti, F., Lustri, A.M., Errico, M.C., Bottero, L., Cannistraci, A., De Feo, A., Petrini, M., Pedini, F., Biffoni, M., et al. (2013). miR-126&126* restored

expressions play a tumor suppressor role by directly regulating ADAM9 and MMP7 in melanoma. PLoS One *8*, e56824.

27. Caporali, S., Amaro, A., Levati, L., Alvino, E., Lacal, P.M., Mastroeni, S., Ruffini, F., Bonmassar, L., Antonini Cappellini, G.C., Felli, N., et al. (2019). miR-126-3p down-regulation contributes to dabrafenib acquired resistance in melanoma by up-regulating ADAM9 and VEGF-A. J. Exp. Clin. Cancer Res. *38*, 272.
28. Koo, T., and Kim, J.S. (2017). Therapeutic applications of CRISPR RNA-guided genome editing. Brief. Funct. Genomics *16*, 38–45.
29. Egli, M., and Manoharan, M. (2019). Re-Engineering RNA Molecules into Therapeutic Agents. Acc. Chem. Res. *52*, 1036–1047.
30. Adams, D., Gonzalez-Duarte, A., O'Riordan, W.D., Yang, C.C., Ueda, M., Kristen, A.V., Tournev, I., Schmidt, H.H., Coelho, T., Berk, J.L., et al. (2018). Patisiran, an RNAi Therapeutic, for Hereditary Transthyretin Amyloidosis. N. Engl. J. Med. *379*, 11–21.
31. Hoy, S.M. (2018). Patisiran: First Global Approval. Drugs *78*, 1625–1631.
32. Guo, C., Sah, J.F., Beard, L., Willson, J.K.V., Markowitz, S.D., and Guda, K. (2008). The noncoding RNA, miR-126, suppresses the growth of neoplastic cells by targeting phosphatidylinositol 3-kinase signaling and is frequently lost in colon cancers. Genes Chromosomes Cancer *47*, 939–946.
33. Cifani, N., Chronopoulou, L., Pompili, B., Di Martino, A., Bordi, F., Sennato, S., Di Domenico, E.G., Palocci, C., and Ascenzioni, F. (2015). Improved stability and efficacy of chitosan/pDNA complexes for gene delivery. Biotechnol. Lett. *37*, 557–565.
34. Amaduzzi, F., Bomboi, F., Bonincontro, A., Bordi, F., Casciardi, S., Chronopoulou, L., Diociaiuti, M., Mura, F., Palocci, C., and Sennato, S. (2014). Chitosan-DNA complexes: charge inversion and DNA condensation. Colloids Surf. B Biointerfaces *114*, 1–10.
35. Chronopoulou, L., Falasca, F., Di Fonzo, F., Turriziani, O., and Palocci, C. (2022). siRNA Transfection Mediated by Chitosan Microparticles for the Treatment of HIV-1 Infection of Human Cell Lines. Materials (Basel) *15*, 5340.
36. Lavertu, M., Méthot, S., Tran-Khanh, N., and Buschmann, M.D. (2006). High efficiency gene transfer using chitosan/DNA nanoparticles with specific combinations of molecular weight and degree of deacetylation. Biomaterials *27*, 4815–4824.
37. Flego, M., Colotti, G., Ascione, A., Dupuis, M.L., Petrucci, E., Riccioni, R., Andreotti, M., Raggi, C., Boe, A., Barca, S., et al. (2021). Isolation and preliminary characterization of a human 'phage display'-derived antibody against neural adhesion molecule-1 antigen interfering with fibroblast growth factor receptor-1 binding. Hum. Antibodies *29*, 63–84.
38. Ascione, A., Arenaccio, C., Mallano, A., Flego, M., Gellini, M., Andreotti, M., Fenwick, C., Pantaleo, G., Vella, S., and Federico, M. (2019). Development of a novel human phage display-derived anti-LAG3 scFv antibody targeting CD8(+) T lymphocyte exhaustion. BMC Biotechnol. *19*, 67.
39. Dowaidar, M., Nasser Abdelhamid, H., Hällbrink, M., Langel, Ü., and Zou, X. (2018). Chitosan enhances gene delivery of oligonucleotide complexes with magnetic nanoparticles-cell-penetrating peptide. J. Biomater. Appl. *33*, 392–401.
40. Faust, J.J., Masserano, B.M., Mielke, A.H., Abraham, A., and Capco, D.G. (2014). Engineered nanoparticles induced brush border disruption in a human model of the intestinal epithelium. Adv. Exp. Med. Biol. *811*, 55–72.
41. Atkins, M.B., Lee, S.J., Chmielowski, B., Tarhini, A.A., Cohen, G.I., Truong, T.G., Moon, H.H., Davar, D., O'Rourke., M., Stephenson, J.J., et al. (2023). Combination Dabrafenib and Trametinib Versus Combination Nivolumab and Ipilimumab for Patients With Advanced BRAF-Mutant Melanoma: The DREAMseq Trial-ECOG-ACRIN EA6134. J. Clin. Oncol. *41*, 186–197.
42. Ascierto, P.A., Mandalà, M., Ferrucci, P.F., Guidoboni, M., Rutkowski, P., Ferraresi, V., Arance, A., Guida, M., Maiello, E., Gogas, H., et al. (2023). Sequencing of Ipilimumab Plus Nivolumab and Encorafenib Plus Binimetinib for Untreated BRAF-Mutated Metastatic Melanoma (SECOMBIT): A Randomized, Three-Arm, Open-Label Phase II Trial. J. Clin. Oncol. *41*, 212–221.
43. Trojaniello, C., Sparano, F., Cioli, E., and Ascierto, P.A. (2023). Sequencing Targeted and Immune Therapy in BRAF-Mutant Melanoma: Lessons Learned. Curr. Oncol. Rep. *25*, 623–634.
44. Narmani, A., Rezvani, M., Farhood, B., Darkhor, P., Mohammadnejad, J., Amini, B., Refahi, S., and Abdi Goushbolagh, N. (2019). Folic acid functionalized nanoparticles as pharmaceutical carriers in drug delivery systems. Drug Dev. Res. *80*, 404–424.
45. Narmani, A., and Jafari, S.M. (2021). Chitosan-based nanodelivery systems for cancer therapy: Recent advances. Carbohydr. Polym. *272*, 118464.
46. Castellani, G., Buccarelli, M., Lulli, V., Ilari, R., De Luca, G., Pedini, F., Boe, A., Felli, N., Biffoni, M., Pilozzi, E., et al. (2022). MiR-378a-3p Acts as a Tumor Suppressor in Colorectal Cancer Stem-Like Cells and Affects the Expression of MALAT1 and NEAT1 lncRNAs. Front. Oncol. *12*, 867886.